Cd-free quantum dot pellets for efficient white light generation

YEMLIHA ALTINTAS,[1] MOHAMMAD YOUNIS TALPUR,[2] AND EVREN MUTLUGÜN[2,*]

[1]*Department of Materials Science and Nanotechnology, Abdullah Gül University, Kayseri, TR-38080, Turkey*
[2]*Department of Electrical-Electronics Engineering, Abdullah Gül University, Kayseri, TR-38080, Turkey*
[*]evren.mutlugun@agu.edu.tr

Abstract: Semiconductor quantum dots have been on demand for niche optoelectronic applications providing color tenability and possessing high quantum yield and high extinction coefficient. Although the investigation of II-VI have attained a mature level of understanding of the photo physical properties, suppression of the nonradiative decay channels and enhancing the optical properties for III-V material systems still remain a challenge. In this study, we have developed and demonstrated a simple, very fast, and efficient strategy to synthesize the highly luminescent III-V group based In(Zn)P quantum dots (QDs) utilized by the effect of core growth temperature, revealing their emission kinetics and their outstanding application for white light generation. Varying the core growth temperature from 240°C to 90°C, limiting the extent of the precursors involved in the synthesis, and a substantial enhancement of the photoluminescence quantum yield up to 75% is demonstrated. Further modification of the synthesis procedure with optimizing the In:P precursor ratio for the first time up to 88.5 ± 5.5% quantum yield of alloyed core/shell In(Zn)P/ZnS QDs is achieved, in which the whole synthesis process takes only around one hour. In addition, as a demonstration of Cd-free pellets, versatile pellets of green and orange emitting QDs within KCl macrocrystals are prepared. Hybridizing with blue LED, a white light with correlated color temperature of 4597K along with an unprecedentedly high color rendering index of 90 is presented.

References and links

1. L. E. Brus, "Electron–electron and electron-hole interactions in small semiconductor crystallites: The size dependence of the lowest excited electronic state," J. Chem. Phys. **80**(9), 4403–4409 (1984).
2. S. Tamang, C. Lincheneau, Y. Hermans, S. Jeong, and P. Reiss, "Chemistry of InP nanocrystal syntheses," Chem. Mater. **28**(8), 2491–2506 (2016).
3. I. Robel, V. Subramanian, M. Kuno, and P. V. J. Kamat, "Quantum dot solar cells. harvesting light energy with CdSe nanocrystals molecularly linked to mesoscopic TiO₂ films," J. Am. Chem. Soc. **128**(7), 2385–2393 (2006).
4. I. Hod, V. González-Pedro, Z. Tachan, F. Fabregat-Santiago, I. Mora-Seró, J. Bisquert, and A. Zaban, "Dye versus quantum dots in sensitized solar cells: participation of quantum dot absorber in the recombination process," J. Phys. Chem. Lett. **2**(24), 3032–3035 (2011).
5. E. Mutlugun, P. L. Hernandez-Martinez, C. Eroglu, Y. Coskun, T. Erdem, V. K. Sharma, E. Unal, S. K. Panda, S. G. Hickey, N. Gaponik, A. Eychmüller, and H. V. Demir, "Large-area (over 50 cm × 50 cm) freestanding films of colloidal InP/ZnS quantum dots," Nano Lett. **12**(8), 3986–3993 (2012).
6. B. Guzelturk, P. L. Hernandez Martinez, Q. Zhang, Q. Xiong, H. Sun, X. W. Sun, A. O. Govorov, and H. V. Demir, "Excitonics of semiconductor quantum dots and wires for lighting and displays," Laser Photonics Rev. **8**(1), 73–93 (2014).
7. X. Gao, L. Yang, J. A. Petros, F. F. Marshall, J. W. Simons, and S. Nie, "In vivo molecular and cellular imaging with quantum dots," Curr. Opin. Biotechnol. **16**(1), 63–72 (2005).
8. M. A. Walling, J. A. Novak, and J. R. Shepard, "Quantum dots for live cell and in vivo imaging," Int. J. Mol. Sci. **10**(2), 441–491 (2009).

9. S. G. Kwon and T. Hyeon, "Formation mechanisms of uniform nanocrystals via hot-injection and heat-up methods," Small **7**(19), 2685–2702 (2011).

10. A. B. Greytak, P. M. Allen, W. Liu, J. Zhao, E. R. Young, Z. Popović, B. Walker, D. G. Nocera, and M. G. Bawendi, "Alternating layer addition approach to CdSe/CdS core/shell quantum dots with near-unity quantum yield and high on-time fractions," Chem. Sci. (Camb.) **3**(6), 2028–2034 (2012).

11. W. Lin, Y. Niu, R. Meng, L. Huang, H. Cao, Z. Zhang, H. Qin, and X. Peng, "Shell-thickness dependent optical properties of CdSe/CdS core/shell nanocrystals coated with thiol ligands," Nano Res. **9**(1), 260–271 (2016).

12. R. C. Page, D. Espinobarro-Velazquez, M. A. Leontiadou, C. Smith, E. A. Lewis, S. J. Haigh, C. Li, H. Radtke, A. Pengpad, F. Bondino, E. Magnano, I. Pis, W. R. Flavell, P. O'Brien, and D. J. Binks, "Near-unity quantum yields from chloride treated CdTe colloidal quantum dots," Small **11**(13), 1548–1554 (2015).

13. M. D. Tessier, D. Dupont, K. D. Nolf, J. D. Roo, and Z. Hens, "Economic and size-tunable synthesis of InP/ZnE (E= S, Se) colloidal quantum dots," Chem. Mater. **27**(13), 4893–4898 (2015).

14. Y. Altıntas, M. Y. Talpur, M. Unlu, and E. Mutlugun, "Highly efficient Cd-free alloyed core/shell quantum dots with optimized precursor concentrations," J. Phys. Chem. C **120**(14), 7885–7892 (2016).

15. U. T. D. Thuy, P. Reiss, and N. Q. Liem, "Luminescence properties of In (Zn)P alloy core/ZnS shell quantum dots," Appl. Phys. Lett. **97**(19), 193104 (2010).

16. J. P. Park, J.-J. Lee, and S.-W. Kim, "Highly luminescent InP/GaP/ZnS QDs emitting in the entire color range via a heating up process," Sci. Rep. **6**, 30094 (2016).

17. T. Otto, M. Müller, P. Mundra, V. Lesnyak, H. V. Demir, N. Gaponik, and A. Eychmüller, "Colloidal nanocrystals embedded in macrocrystals: robustness, photostability, and color purity," Nano Lett. **12**(10), 5348–5354 (2012).

18. M. Müller, M. Kaiser, G. M. Stachowski, U. R. Genger, N. Gaponik, and A. Eychmüller, "Photoluminescence quantum yield and matrix-induced luminescence enhancement of colloidal quantum dots embedded in ionic crystals," Chem. Mater. **26**(10), 3231–3237 (2014).

19. M. Adam, Z. Wang, A. Dubavik, G. M. Stachowski, C. Meerbach, Z. S. Erdem, C. Rengers, H. V. Demir, N. Gaponik, and A. Eychmüller, "Liquid-liquid diffusion-assisted crystallization: A fast and versatile approach toward high quality mixed quantum dot- salt crystals," Adv. Funct. Mater. **25**(18), 2638–2645 (2015).

20. M. Adam, T. Erdem, G. M. Stachowski, Z. Soran-Erdem, J. F. L. Lox, C. Bauer, J. Poppe, H. V. Demir, N. Gaponik, and A. Eychmüller, "Implementation of high-quality warm-white light-emitting diodes by a model-experimental feedback approach using quantum dot–salt mixed crystals," ACS Appl. Mater. Interfaces **7**(41), 23364–23371 (2015).

21. Y. Altıntas, A. F. Yazici, M. Unlu, S. Dadi, S. Genc, and E. Mutlugün, "Excitonic interaction amongst InP/ZnS salt pellets," J. Mater. Chem. C Mater. Opt. Electron. Devices **5**, 7328–7336 (2017).

22. J. Ziegler, S. Xu, E. Kucur, F. Meister, M. Batentschuk, F. Gindele, and T. Nann, "Silica-coated InP/ZnS nanocrystals as converter material in white LEDs," Adv. Mater. **20**(21), 4068–4073 (2008).

23. L. Li and P. Reiss, "One-pot synthesis of highly luminescent InP/ZnS nanocrystals without precursor injection," J. Am. Chem. Soc. **130**(35), 11588–11589 (2008).

24. Y. Altıntas, M. Y. Talpur, and E. Mutlugün, "Efficient Förster resonance energy transfer donors of In(Zn)P/ZnS quantum dots," J. Phys. Chem. C **121**(5), 3034–3043 (2017).

25. A. Benad, C. Guhrenz, C. Bauer, F. Eichler, M. Adam, C. Ziegler, N. Gaponik, and A. Eychmüller, "Cold flow as versatile approach for stable and highly luminescent quantum dot–salt composites," ACS Appl. Mater. Interfaces **8**(33), 21570–21575 (2016).

26. M. Grabolle, M. Spieles, V. Lesnyak, N. Gaponik, A. Eychmüller, and U. R. Genger, "Determination of the Fluorescence Quantum Yield of Quantum Dots: Suitable Procedures and Achievable Uncertainties,"," Anal. Chem. **81**(15), 6285–6294 (2009).

27. J. R. Lakowicz, "Principles of Fluorescence Spectroscopy," 3rd Eds.; Springer: US, pp. XXVI, 954 (2007).

28. F. Pietra, L. De Trizio, A. W. Hoekstra, N. Renaud, M. Prato, F. C. Grozema, P. J. Baesjou, R. Koole, L. Manna, and A. J. Houtepen, "Tuning the lattice parameter of In_xZn_yP for highly luminescent lattice-matched core/shell quantum dots," ACS Nano **10**(4), 4754–4762 (2016).

29. C. J. Bridge, P. Dawson, and P. D. Buckle, "Photoluminescence spectroscopy and decay time measurements of polycrystalline thin film CdTe/CdS solar cells," J. Appl. Phys. **88**(11), 6451–6456 (2000).

30. C. Galland, Y. Ghosh, A. Steinbrück, J. A. Hollingsworth, H. Htoon, and V. I. Klimov, "Lifetime blinking in nonblinking nanocrystal quantum dots," Nat. Commun. **3**, 908 (2012).

31. C. Galland, Y. Ghosh, A. Steinbrück, M. Sykora, J. A. Hollingsworth, V. I. Klimov, and H. Htoon, "Two types of luminescence blinking revealed by spectroelectrochemistry of single quantum dots," Nature **479**(7372), 203–207 (2011).

32. M. Banski, M. Afzaal, M. A. Malik, A. Podhorodecki, J. Misiewicz, and P. O. Brien, "Special Role for Zinc Stearate and Octadecene in the Synthesis of Luminescent ZnSe Nanocrystals," Chem. Mater. **27**(11), 3797–3800 (2015).

33. T. Mishra, R. K. Sahu, S.-H. Lim, L. G. Salamanca-Riba, and S. Bhattacharjee, "Hexadecylamine Capped Silver and Gold Nanoparticles: Comparative Study on Formation and Self- Organization," Mater. Chem. Phys. **123**(2–3), 540–545 (2010).

1. Introduction

Since their first appearance in 80s, semiconductor quantum dots (QDs) have been on the spot serving for the energy efficient applications [1]. The ease in the modification of their optical properties by changing the chemical composition or size, altering their functionalization by the modification of the functional ligand groups attached, and the versatility in their processing (i.e., solution process-ability) have made them promising alternative agents when compared to epitaxial grown nano structures [2]. Thanks to their narrow emission profile and high photoluminescence quantum yield, these particles have started to take part in the development of the high- end technology, on one side serving as energy harvesting agents for solar energy applications [3, 4] and white light generation [5, 6], on the other hand acting for in vivo imaging in biotechnology [7, 8]. Along with the efforts on the chemical synthesis, the methods of "heating up" or "hot injection" have been found to be leading routes for the synthesis of these particles [9]. As the quantum confinement mechanism taken into account, the efficient carrier confinement at the nano-scale core is achieved by means of using a wide band gap material, by suppressing the nonradiative decay channels in the recombination process. With the synthesis approaches and recipes developed, the materials of the II-VI semiconductor family, including CdSe [10, 11] and CdTe [12] quantum dots have now been established to possess near unity quantum yield and narrow size distribution. However, InP based quantum dots suffer from the lower quantum yield and wider emission spectral bandwidth as compared to CdSe based counterparts. In the literature, Tessier et.al, demonstrated the color tunable InP/ZnS and InP/ZnSe quantum dots in the range of 510-630 nm with emission band width of 46-63 nm, using indium halide and aminophosphine precursors [13].

In their report the measured quantum yield is given as 79% (maximum) for the particles possessing 70 nm full width at half maximum (FWHM) value. Regarding the efforts in achieving QDs with narrow FWHM, our group recently demonstrated InPZnS alloyed core/ZnS shell quantum dots with up to 45nm FWHM value and quantum efficiency level of 78% [14]. Thuy, et al. reported In(Zn)P/ZnS shell quantum dots with quantum yield in the range of 60-70% [15]. Using heating up method, InP/GaP/ZnS QDs have been achieved with quantum efficiency reaching 85% [16]. This is one of the highest reported quantum yield value thus far for InP based materials. Although various methods and recipes have been employed in order to reveal the emission kinetics and mechanisms of the InP/ZnS quantum dots, the effect of hot injection temperature for these material systems have not been investigated thus far.

In addition to the efforts in the synthesis of QDs, the investigations of their solid state forms also attain considerable interest from the application point of view. Recently, there has been a great interest in embedding QDs in macrocrystals [17, 18]. The macrocrystals of QDs have been shown to provide passivation of colloids from the environment and enhance thermal and photo stability of the QDs. A new era of QD powders [17–21] to open up new possibilities for the use for optoelectronics.

In that regards, in this report we demonstrate the synthesis of very efficient In(Zn)P/ZnS QD by the investigation of hot injection temperature and utilize them for the generation of white light with unprecedentedly high color rendering index of 90. As an important investigation of the effect of the hot injection temperature, we have varied the growth temperature of the synthesized quantum dots systematically from 240 °C to 90 °C. Decreasing the P-precursor injection temperature has provided us achieve narrower FWHM and higher photoluminescence quantum yield reaching 75%. At temperatures less than 90 °C, the P-precursor is not reacted sufficiently to provide nucleation and growth of quantum dots. Further optimizing the recipe by modifying the In:P precursor ratio and other precursors involved, we have achieved QDs with very high quantum yield, i.e. 88.5 ± 5.5%. Our results have also been monitored using the time resolved photoluminescence measurements.

In addition, as a potential application of these colloidal QDs, we have incorporated them with salt macrocrystals and fabricated versatile pellets of Cd-free quantum dots. In a hybrid approach with inorganic blue LED, the white light generated possesses an unprecedentedly high color-rendering index of 90, along with correlated color temperature of 4597K.

2. Experimental

2.1 Chemicals and reagents

Indium chloride (InCl$_3$, 98%), stearic acid (CH$_3$(CH$_2$)$_{16}$COOH, 98.5%), Zinc undecylenate ([H$_2$C = CH(CH$_2$)$_8$CO$_2$]$_2$Zn, 98%), Hexadecylamine (CH$_3$(CH$_2$)$_{15}$NH$_2$, 98%), 1-octadecene (C$_{18}$H$_{36}$, 90%), tris(trimethylsilyl)phosphine ([(CH$_3$)$_3$Si]$_3$P, 95%),, Cyclohexyl isothiocyanate (C$_6$H$_{11}$NCS, 98%), hexane (C$_6$H$_{14}$, 95%), acetone ((CH$_3$)$_2$CO, 99.5%)and methanol (CH$_3$OH, 99.8%), Potassium chloride (KCl, ≥99%). The chemicals and reagents were obtained from Sigma Aldrich and used without further purification.

2.2 Characterization

Photoluminescence (PL) characterizations were carried out using Agilent-Cary Eclipse fluorescence spectrophotometer. UV-Vis spectroscopy was performed using Shimadzu 1800 and Thermo Genesys 10S spectrometer. Time resolved photoluminescence (TRPL) characterization were conducted with Pico Quant FluoTime 200 equipped with 375 nm pulsed laser diode, Transmission electron microscope (TEM) images and Energy-dispersive X-ray spectroscopy (EDX) analysis were carried out employing a FEI Tecnai G2 F30 and XRD by PANalytical: X'pert Pro MPD. Fourier Transform Infrared Spectroscopy (FTIR) were performed using Thermo Scientific Nicolet-6700 and white LED characterizations were carried out using fiber coupled StellarNet Inc. Spectrometer and Konika Minolta LS150 Luminancemeter.

2.3 QD Synthesis methods

2.3.1 Method-1

In a typical synthesis for the core and shell materials, we have followed and modified the recipe outlined by Nann and associates [22], Indium chloride (0.1 mmol), stearic acid (0.1 mmol), hexadecylamine (0.2 mmol) and zinc undecylenate (0.08 mmol) were mixed in 1-Octadecene (3 ml) into the three-necked flask and degassed (under vacuum) at room temperature for 5 minutes. Then, Argon (Ar) gas flow has been maintained and the flask is quickly heated to the elevated temperature, at which the solution of tris (trimethylsilyl) phosphine (P(TMS)$_3$) is introduced to the reaction P(TMS)$_3$ precursor solution was prepared inside the glove box by mixing (0.1 mmol, 29 μL) of (P(TMS)$_3$) in 1-octadecene (0.5 mL). When temperature is maintained at a given set temperature, the P-precursor (P(TMS)$_3$) is rapidly injected to the flask during vigorous stirring and the system is kept at that temperature for 20 minutes. After that, the core solution was cooled down to room temperature and ready for shell process.

For the growth of ZnS shell, Zinc undecylenate (0.3 mmol) was added into the previously prepared quantum dot solution at room temperature. The solution was maintained under vacuum for 5 minutes to remove the moisture and oxygen from the system. Afterwards, the solution is heated to 220 °C under Ar gas atmosphere. When temperature of the solution reached to 220 °C, then cyclohexyl isothiocyanate solution (0.15 mmol) in ODE (1mL) was introduced to the system by syringe pump at 10ml/hour rate. The solution was stirred vigorously at 220 °C for 20 minutes. Finally, it was cooled down to room temperature for further purification process of synthesized QDs and 5 ml of hexane added. The mixture of as synthesized QDs was precipitated by centrifugation (5000 rpm, 5 min) to remove any insoluble residues and then the particles have been crashed out by adding acetone and methanol followed by centrifugation (5000 rpm, 15 min). The process has been repeated for

two times and the purified quantum dots are dissolved in fresh hexane. It is worth noting here that for the optimization of the cleaning process; after separation of by-product in the synthesis, instead of one times precipitation with adding acetone and methanol together, the first precipitation can be carried out by acetone addition (1:2 by volume) and the precipitate may be discarded. This first step precipitations allow us to remove unreacted species and also enable size selective precipitation, which provides us settle the larger sized particles with low quantum yield. By this approach, large and inefficient QD particles are separated from the first precipitation. The supernatant then is to be precipitated by methanol addition and centrifugation, which would provide particles with better size distribution and higher emission characteristics. Finally, the purified quantum dots are dissolved in fresh hexane.

2.3.2 Method-2

Different from Method 1, we have focused on the optimization of In:P ratio and Zn concentration and ligand concentration in general. In our previous study [14], quantum efficiency of synthesized In-based Cd-free QDs increased with increasing of In/P ratio. In that study, In/P ratio changed from 0.8 to 1.4 and QE of obtained nanocrystal's increased from 41% to 61%. Therefore in Method 2, In/P ratio has been changed from 1 to 1.4. For the In to ligand ratio, a ratio of 1:3 has been implemented, which has also been to be optimal for In based synthesis [23]. The kind and concentration of Zn-precursor also affect the quality of InZnP/ZnS QDs [24]. The concentration of Zn-precursor increased from 0.1 mmol to 0.12 mmol allowing for an optimized Zn amount at the core growth stage. In addition, the solvent Octadecene has been increased from 3 ml to 4 ml in Method 2 in order to control the core growth rate. Also shell growth temperature has been increased from 220 °C to 230 °C which is the most convenient temperature for the formation of ZnS shell materials especially in InP core nanocrystal. Shell growth time also increased to 30 min.

In this synthesis method, $InCl_3$ (0.12 mmol), SA (0.12 mmol), HDA (0.24 mmol) and zinc undecylenate (0.12 mmol) were loaded in ODE (4mL) into the three-necked flask and degassed at room temperature (under vacuum) for 5 minutes. Then, the reaction was kept under Ar gas flow and quickly heated up to 90 °C. The solution of tris (trimethylsilyl) phosphine $(P(TMS)_3)$ ((24.65 µL, 0.085 mmol) in 0.5 mL ODE) was introduced to the reaction flask swiftly under vigorous stirring and particle growth continued for 20 minutes at 90 °C. Finally, the reaction was rapidly cooled down to room temperature.

In this shell process, precursor's concentrations of zinc undecylenate and cyclohexyl isothiocyanate were same as previously described in shell process (Method-1), with the only variation of temperature and waiting time for shell growth process. The temperature for shell growth was used at 230 °C and kept for 30 min. The purification process of the QDs was performed same as discussed earlier in (Method-1).

2.4 Preparation of QD macrocrystal pellet

In the preparation of the QD macrocrystals pellet, we have used the modified recipe of QD salt preparation outlined in literature [21, 25]. After milling process, 0.5 g KCl salt was mixed with hexane (1 ml), and orange emitting (75 µl) and green emitting (50 µl) QDs dissolved in hexane (corresponding to green:orange PL intensity ratio 3:1). The solution was stirred 45 minute under room temperature. In order to obtain the powder QD-salt, the mixture was dried under vacuum assisted desiccator for 30 min. QD salt powder was compressed with Specac hydrolic pressure system (applying 10 ton per c.a.1 cm^2) and prepared pellets were stored under desiccator to prevent from moisture. The pellet prepared with 500 mg KCl is 13 mm in diameter and 1.94 mm in thickness.

3. Results and discussion

The optical properties of the synthesized quantum dots are given in Fig. 1. The colloidal quantum dot synthesis recipe has been studied and developed using the recipe in the

literature, given in Methods section. Unless otherwise stated, core quantum dots have further been coated with the same ZnS shell coating, using recipe outlined in the manuscript. Figures 1(a) and 1(b) show the spectra by changing of the core injection and growth temperature systematically from 240 °C to 90 °C, we have observed the blue-shift of the first excitonic peak and peak emission wavelength of the nanocrystals. The injection of the tristrimethylsilyl phosphine precursor at lower temperatures has changed the growth kinetics of the particles, influencing the emission properties and optical quality of the particles. By lowering the core growth temperatures, the peak emission wavelength has down shifted from 621 to 508 nm, along with quantum yield increasing from 18% to 75%. Figure 1(c) depicts the change in FWHM, peak emission wavelength and quantum yield as a function of core injection temperature.
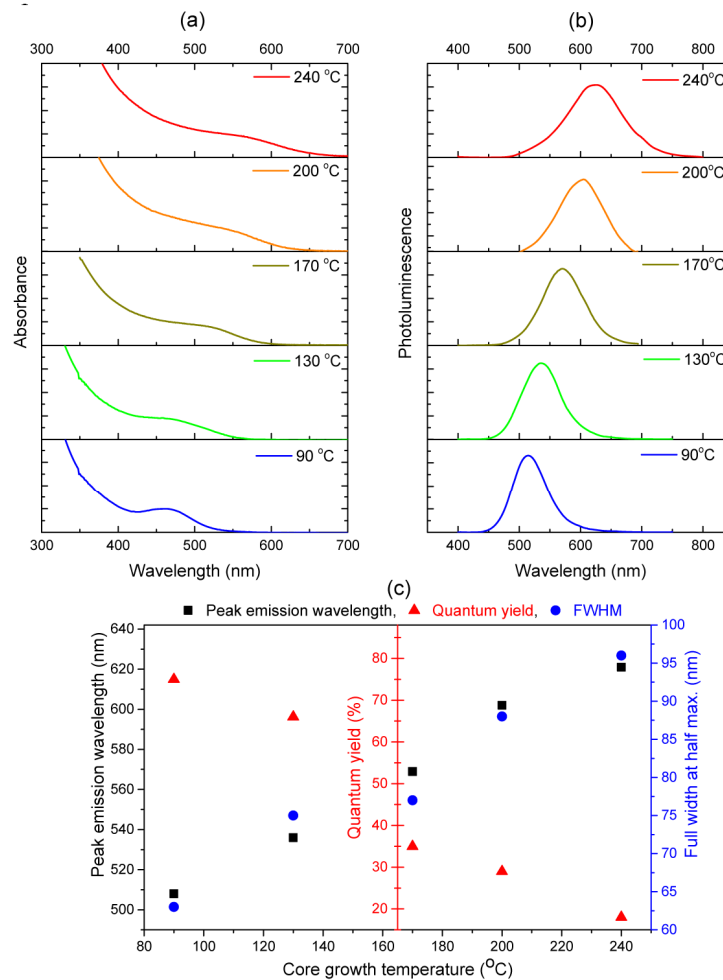
Fig. 1. (a) Absorption spectrum of alloyed core/shell In(Zn)P/ZnS QDs at different temperatures. (b) Photoluminescence spectrum of alloyed core/shell In(Zn)P/ZnS QDs at different temperatures. (c) Peak emission wavelength, quantum yield and full width-half maximum for alloyed core/shell In(Zn)P/ZnS QDs as a function of core growth temperature.

The experimental value of the quantum efficiency for the alloyed core/shell In(Zn)P/ZnS QDs have been measured by comparing with organic dye [26], Rhodamine 6G, having quantum efficiency of 95% (dissolved in absolute ethanol), using Eq. (1).

$$QE_s = QE_r \frac{I_s A_r n_s^2}{I_r A_s n_r^2} \tag{1}$$

Here subscripts "*s*" and "*r*" stands for the sample and reference respectively, "QE" stands for quantum efficiency, *"I"* represent the integrated photoluminescence intensity, *"A"* represents absorbance value and "*n*" stands for the refractive index of the solvent (ethanol for the respective dye and n-hexane for the QD solvent).

The full width half maximum values of the colloidal quantum dots have decreased from 96 to 63 nm, which is shown to be correlated with the photoluminescence quantum yield values. The optical properties discussed have further been summarized in Table 1.

Table 1. Photoluminescence peak emission wavelength, quantum yield, emission full width half maximum value and core growth temperature for cyan, green, yellow, orange and red emitting In(Zn)P/ZnS quantum dots. (The measured quantum yield values vary ± 5%, depending on the excitation wavelength of the QDs)

Parameters	Cyan	Green	Yellow	Orange	Red
PL peak emission wavelength (nm)	508	536	569	602	621
Quantum yield (%)	75	66	35	29	18
FWHM (nm)	63	75	77	88	96
Core growth temperature (°C)	90	130	170	200	240

Regarding the emission quality of the nanocrystals formed with hot injection method, the observation of the increase in quality of the alloyed core/shell In(Zn)P/ZnS QDs with decreasing the core injection temperature has systematically been shown. In order to understand the origin of this behavior, emission kinetics of the alloyed core/shell QDs have been investigated by time correlated single photon counting method. As has been shown in Fig. 2, we observed the suppression of the trap states by using lower temperatures for precursor injection, which is critically important to suppress the nonradiative decay channels. In agreement with the observation of the enhanced photoluminescence quantum yield, the time correlated single photon counting measurements have also shown to reflect the nonradiative decay channels being more dominant for the case of quantum dots with growth temperatures higher than 90 °C. We have observed faster lifetime decay components becoming more dominant as the core growth temperature have been increased.
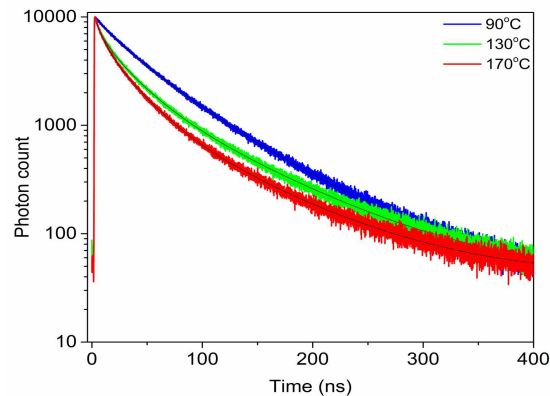

Fig. 2. Time correlated single photon count decays for alloyed core/shell In(Zn)P/ZnS quantum dots as a function of core growth temperature.

The decay curves have been fit with 3-exponentials using the intensity-weighted lifetime as given in Eq. (2) [27].

$$\tau_{int} = \sum_i \frac{A_i \tau_i^2}{A_i \tau_i} \qquad (2)$$

We have calculated the intensity weighted average lifetime to change from 51.81 ns in case of 170 °C, to 71.47 ns for particles grown at 90 °C core growth temperature (Table 2). Due to the low quantum yield and wide FWHM value of the particles synthesized at 200 °C and 240 °C growth temperature, their analysis have not been included in Fig. 2.

Table 2. Photoluminescence decay coefficients and corresponding lifetime values for In(Zn)P/ZnS quantum dots synthesized by varying the core growth temperature.

Core growth temperature	τ_1(ns)	τ_2 (ns)	τ_3 (ns)	$\tau_{average}$(ns) (intensity)	χ^2
90 °C	169.05 ± 2.91 (16.98%)	55.84 ± 0.27 (72.69%)	21.17 ± 0.79 (10.34%)	71.47	1.00
130 °C	83.74 ± 0.56 (57.6%)	27.23 ± 0.34 (37.82%)	6.90 ± 0.57 (4.58%)	58.85	1.03
170 °C	82.86 ± 0.72 (46.71%)	27.34 ± 0.31 (45.97%)	7.38 ± 0.45 (7.32%)	51.81	1.03

As have been explained in the Methods section, the synthesis starts with the formation of the alloyed core structure (In(Zn)P) rather than a regular core of InP. The addition of Zn at the core stage has previously been shown to enhance the optical properties of the nanocrystals, decreasing the lattice mismatch with the shell material to be over coated [15, 28]. Within this scope, the alloyed core including the hexadecylamine and stearic acid ligands as well as indium and zinc precursors have been dissolved and then the P-precursor (tristrimethylsilyl-phosphine) is introduced to the reaction flask at different temperatures (see Method 1).

In order to the understand the origin of the effect of temperature on the alloyed core structure, we have done some further characterizations at the core growth stage without shell coating. Alloyed core structure (In(Zn)P) is characterized with absorbance, steady state PL measurement and EDX analysis which are given in Fig. 3. In that respect we have seen that, the particles having low precursor injection temperatures have pronounced absorption peaks as shown in Fig. 3(a). Also we observe that their absorption and emission spectra are blue shifted as compared to their final shell coated structures (Fig. 3b and Fig. 1). Regarding the elemental composition, carrying out the energy dispersive X ray analysis, Fig. 3c shows the elemental composition of the core core sample of which the injection temperature is 90 °C. It has been shown that the P content of the core is is lower than the In. This is in agreement with our previous finding that the In-rich content provides particles with higher quantum yield [14]. Upon the formation of the alloyed core, the particles shown in Fig. 3d are coated with wider band gap ZnS shell material. The thick shell content employed has a clear influence on the quality of the synthesized particles.
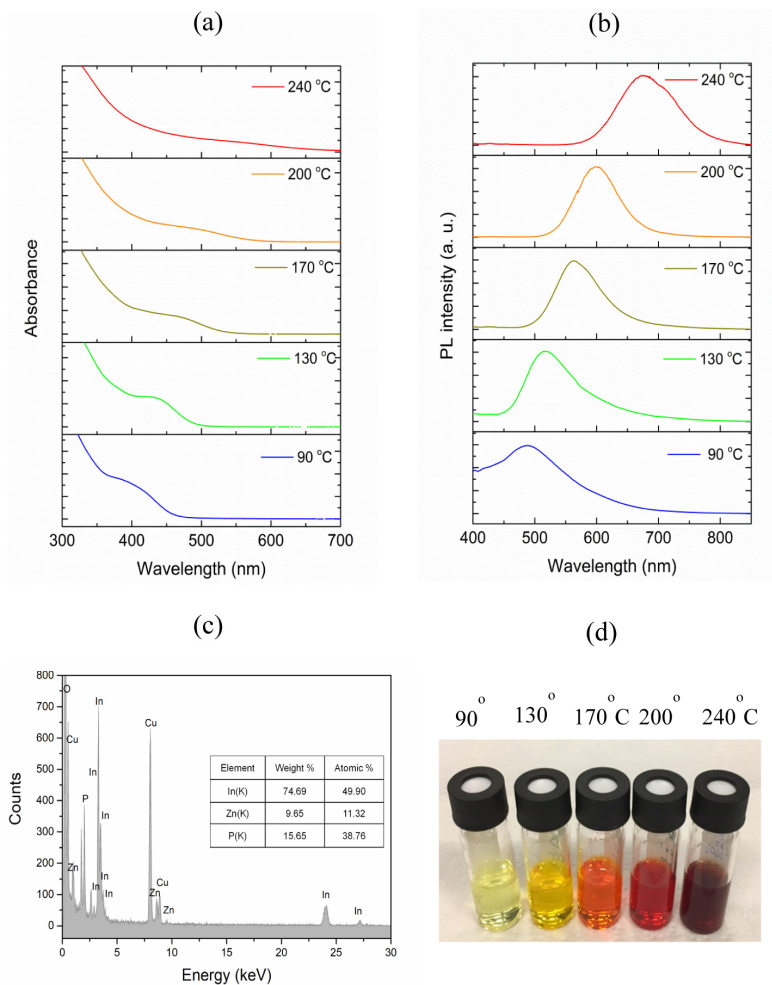
Fig. 3. (a) Absorption, (b) emission spectra of alloyed core In(Zn)P QDs, (c) EDX analysis of alloyed core In(Zn)P QDs which has 90 °C core growth temperature, (d) Photo under daylight for different core growth temperature alloyed core In(Zn)P QDs.

Having observed the effect of particles' emission quality on the core growth temperature, we have worked on achieving particles with higher optical performance, optimizing the synthesis for the particles with core growth temperature of 90 °C. In that regards, we have increased the shell coating temperature from 220 °C to 230 °C allowing for more time for the shell coating, and we have tried our optimization route with changing the In:P ratio in the synthesis, namely using even less P precursor per In employed. Carrying out the synthesis work with P:In ratio as 0.071:1 as compared 1:1, which have been used previously in Method 1, we have seen a substantial enhancement on the emission quality of the particles. The redshift of the peak emission wavelength with lowering the P ratio is in agreement with our previous work [14]. The details of the synthesis of high efficiency particles have been detailed in the Methods section1.

Figure 4 presents the optical properties of the highly efficient particles synthesized at 90 °C. The peak emission wavelength has been found to be 523 nm, along with FWHM value of 68 nm. (It is worth noting here that the excitation wavelength of the emitters has an influence on the FWHM and peak emission wavelength.) The particles synthesized with the Method 2 outlined in the manuscript have record high quantum yield as compared with reference dye,

and do not possess significant degradation in their emission even after more than one year at + 4 °C shelf life. Figure 4(a) presents the absorption and photoluminescence spectra of the synthesized particles and Fig. 4(b) depicts the photoluminescence excitation spectrum which resembles the absorption profile. For the photoluminescence and photoluminescence excitation measurements, a photoluminescence spectrometer (Agilent-Eclipse) with Xe flash lamp equipped with monochromator on excitation and emission window end has been used. The monochromators allow for tuning the excitation wavelength precisely using built in slits as narrow as 1.5 nm and scanning the emission spectra through 190 - 1100 nm window. The photoluminescence measurement has been carried out by exciting the sample at determined excitation wavelength and scanning through the visible, whereas the photoluminescence excitation measurement has been operated by selecting the emission peak wavelength and scanning the excitation spectra through the high energy spectra. It is also worth noting here that apart from the early reports by other groups which takes around 6 hours of reaction time and up to 80% quantum yield [13], the approach presented in this work provided the whole synthesis process to complete within approximately 1 h time, in a simple way, which is considered to be crucial for the large scale integration of the whole system; yielding particles with narrow FWHM and higher quantum efficiency.

In order to understand the origin of the high quantum yield, we have performed time resolved photoluminescence measurement of the synthesized particles. The decay of the photon count has been fit with double exponentials and the decay curve is depicted in Fig. 4(c). High resolution transmission electron microscopy (HR-TEM) image for record high efficiency of alloyed core/shell In(Zn)P/ZnS QDs is given in Fig. 4(e).
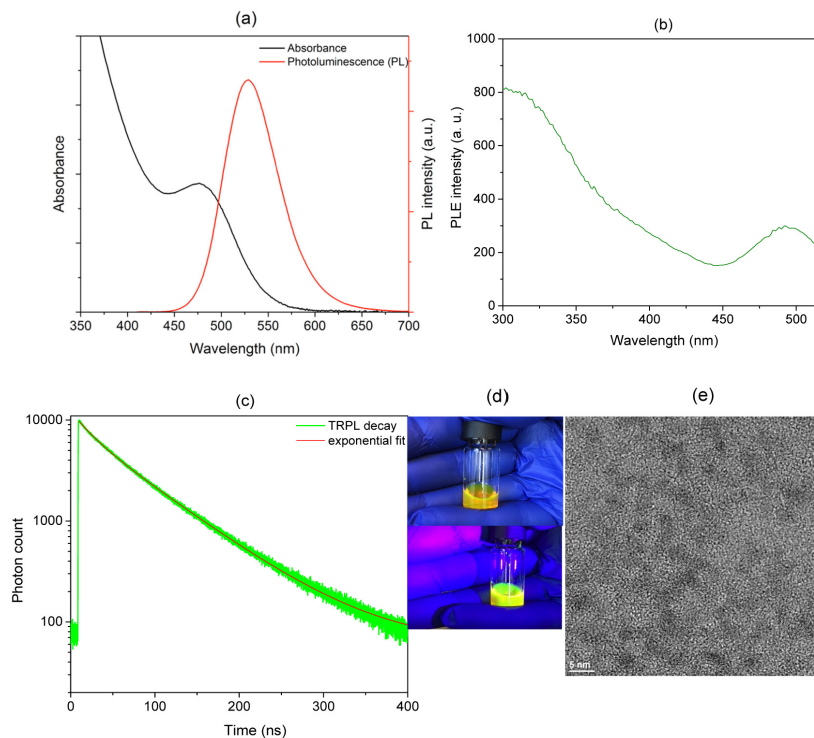

Fig. 4. (a) Absorption and emission spectra, (b) Photoluminescence excitation spectrum, (c) Time resolved photoluminescence spectrum, (d) Photo (up) under daylight, (down) under UV illumination, (e) High resolution transmission electron microscopy image for record high efficiency of alloyed core/shell In(Zn)P/ZnS QDs.

Amplitudes and corresponding lifetime components of record high efficiency In(Zn)P/ZnS QDs has been given in Table 3. The fractional intensities of the positive decay components, extracted from the FluoFit software (PicoQuant) is given as 91.35% for the long decay component (72.07 ns) and 8.65% for the short lifetime (21.08 ns) component.

Table 3. Amplitudes and corresponding lifetime components calculated for In(Zn)P/ZnS quantum dots, synthesized by Method 2

A_1	τ_1 (ns)	A_2	τ_2 (ns)	Intensity weighted lifetime (ns)	χ^2
7264.3 ± 37.1	72.07 ± 0.28 (91.35%)	2351.3 ± 93.5	21.08 ± 0.97 (8.65%)	67.66	1.04

The lifetime components both include radiative and nonradiative decays, and in general the short-lived component correspond to the Auger recombination in QDs, which are known to be non-radiative. Therefore, hypothetically the fast component may be attributed to the nonradiative recombination process owing to the short-lived Auger recombination lifetime [29–31]. In our analysis, we have observed that the short lifetime component only accounts for the 8.65% fractional intensity of the positive decay components. The 91.35% contribution, stemming from the radiative decay has confirmed the achievement of alloyed core/shell In(Zn)P/ZnS QDs with very high quantum yield.

FTIR has been utilized in order to investigate the surface functional groups of the quantum dots. Figure 5(a) presents the specific functional groups corresponding to the wave-numbers by FTIR spectroscopy. The observed wave-numbers corresponding to specific functional groups have been attributed to 722.69 ($-CH_2$ asymmetric rock), 909.27($-C = H$ vinyl), 992.68 (C-N stretching), 1464.67 ($-CH_2$ bending) of aliphatic chain, 1544.70(COO$^-$ stretching) of carboxylate anions and zinc existence for QDs, 1641.61 (N-H bending, with good agreement to isothiocyanate group in shell process), 2853.16 ($-CH_2$ stretching), 2921.63($-CH_3$ stretching) of alkyl chain, 3077.35($-CH = CH_2$ stretching), and 3329.98 cm^{-1}(N-H stretching, with good agreement to isothiocyanate group in shell process), as presented in Fig. 5(a) [14, 32, 33]. In order to understand the crystal structure of the synthesized quantum dots, XRD have been used and corresponding peaks at 27.25, 45.58 and 54.50 degrees are assigned to (111), (220) and (311) planes of the zinc blende structure [22], which has been shown in Fig. 5(b). HR-TEM image for the In(Zn)P/ZnS alloyed core/shell quantum dots, which indicates epitaxial growth of shell due to the zinc-blende structure as shown in Fig. 5(c). The average size of the synthesized alloyed core/shell nanocrystals was determined by TEM at 2.8 ± 0.2 nm. EDX analysis of record high efficiency of alloyed core/shell InZnP/ZnS QDs is given in Fig. 5(d).
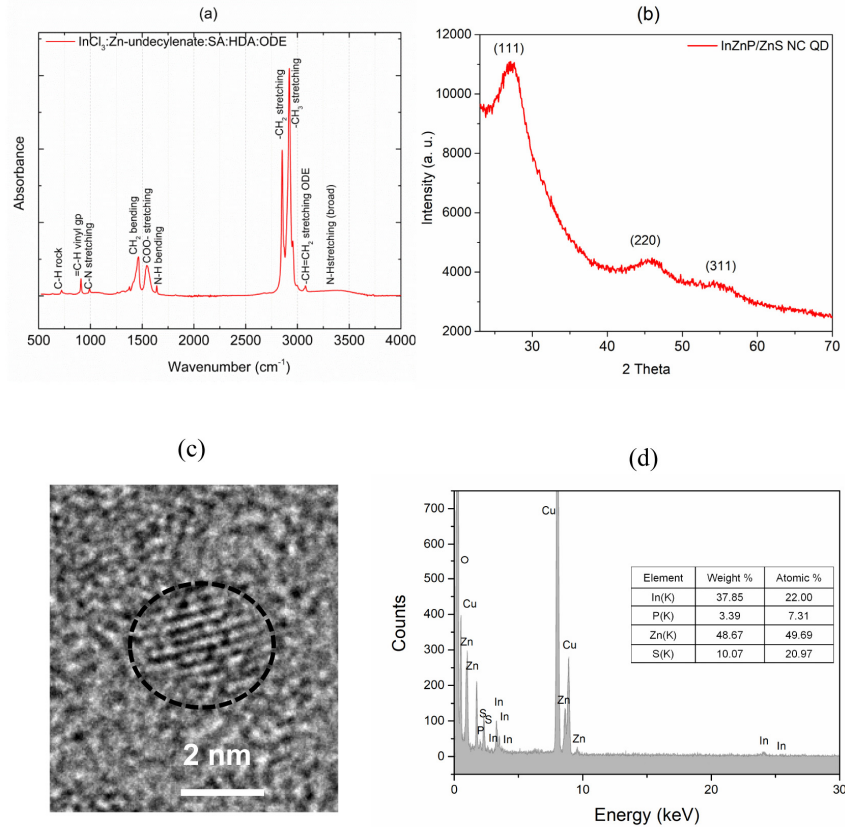
Fig. 5. (a) Fourier transform infrared spectra of alloyed core/shell In (Zn)P/ZnS QDs. (b) X-ray diffraction spectrum alloyed core/shell InZnP/ZnS QDs. (c) High resolution transmission electron microscopy image, (d) EDX analysis for record high efficiency of alloyed core/shell InZnP/ZnS QDs.

In order to generate white light using colloidal alloyed core/shell QDs, green and orange emitting QDs were mixed with KCl and prepared powder form of the salt have been stacked to form the pellet structure, as shown in Figs. 6(a) and 6(b). The details of the preparation of the QD pellet with the KCl salt are outlined in the Methods section. The prepared pellet is hybridized with commercially available InGaN blue LED in order to generate the white light, as presented in Fig. 6(c). Electroluminescence spectrum of the blue LED is shown Fig. 6(d). Starting with their emission intensity level of 1:1, we have systematically vary the ratio of the green and orange emitter ratio in order to achieve an optimal white light spectra, which is found to be on the order of 3:1 for the green to orange emitter. The observed output light spectrum using 3:1 concentration ratio as given in Fig. 6(e) is attributed to the nonradiative energy transfer from green to orange QDs, physically in close proximity in their pellet architecture. The blue LED is operated under 2.75 V and the output light is collected using a fiber-coupled spectrometer. The overall spectrum has been analyzed and found to generate white light with color coordinates of *(x,y) (0.358, 0.361)*. The correlated color temperature corresponding the color coordinates is 4597 K and the calculated color rendering index (CRI) is 90 (calculation done through software available at (http://www.graham.auld.me.uk/406/Calculating CRI-CAM02UCS-v2.xls). The high CRI stems from the use of spectrally wide emitters along with their balanced ratio to act as an optimal lighting source, as shown in Fig. 6(e).
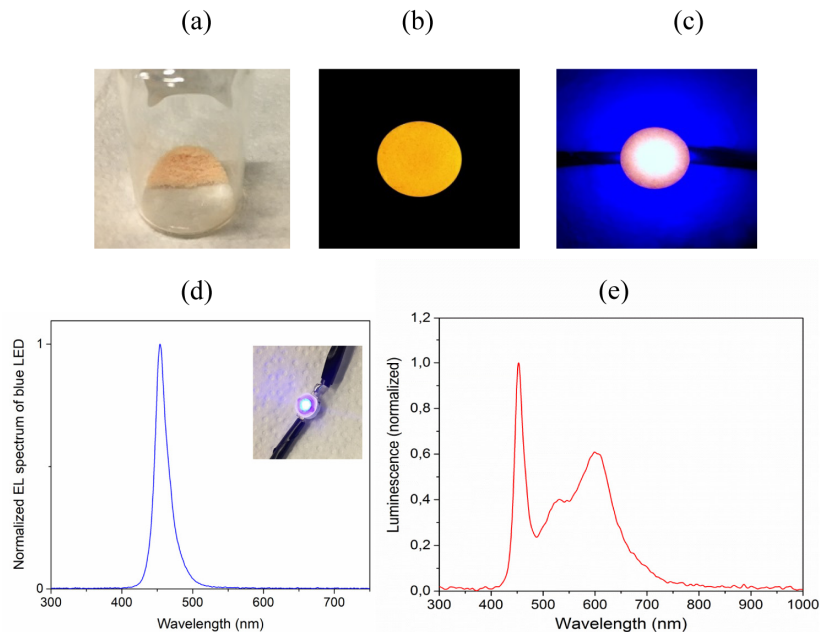
Fig. 6. (a) Photograph of powder form of prepared KCl salt blended with green and orange emitting QDs. (b) Prepared pellet under UV exposure. (c) QD pellet hybridized with InGaN blue LED under operation. (d) Electroluminescence emission spectrum of blue LED, (e) Spectra of the QD pellet hybridized with InGaN blue LED under operation.

Brightness of the blue LED is tested by Konica Minolta LS-150 luminance-meter without and with quantum dots embedded in a salt pellet which is prepared with 500 mg KCl salt. Luminance of blue LED decreased from 278 cd/m^2 to 43.73 cd/m^2 after pellet hybridization. When we prepared a new pellet with 300 mg KCl, thickness of the pellet decreases from 1.94mm to 1.2mm and the brightness of the blue LED decreased from 278 cd/m^2 to 136 cd/m^2 in same experimental setup. The efficiency of the blue LED is observed to increase with a decrease in pellet thickness. Upon these studies, we see that the optimization of the KCl concentration and quantum dot concentration can lead to a white light with desired optical characteristics.

4. Summary and conclusion

In conclusion, we have revealed the effect of the emission kinetics of the In(Zn)P/ZnS quantum dots by modifying the core growth temperature systematically from 240 °C to 90 °C. We have observed that decreasing the core growth temperature substantially enhances the optical quality of the synthesized particles yielding quantum yield up to 75%. Carrying out the research efforts, mainly with optimizing the In:P precursor ratio, we have achieved In(Zn)P/ZnS quantum dots with up to 88.5 ± 5.5% quantum yield, as the first time demonstration of record high efficiency for this material system. The observed high quantum yield with lowering the core growth temperature is attributed to partial decomposition of the P-precursor at low temperature, which provides relatively rich In surface (high In:P ratio), which has systematically influenced the quantum yield value. Besides the structural characterization, the emission kinetics has been investigated using time resolved photoluminescence measurements. It was shown that the radiative decay contributes to the 91.35% of the fractional intensity of the decay components. In an effort to utilize these emitters for the generation of white light, we demonstrate InP based QDs in their pellet architecture and have achieved correlated color temperature of 4597 K and color rendering

index of 90. The achievement of the record high efficiency alloyed core/shell In(Zn)P/ZnS QDs using a simple and fast process, the results presented for the effect of the hot injection temperature, as well as the particles' application to white light emitting diodes in their pellet form are believed to open up new possibilities and prospects for the future applications of III-V colloidal quantum dots.

Competing financial interests

The authors declare no competing financial interest.